



## Article

# Mapping of *Gynaephora alpherakii* Inhabitability Area in the National Park of Qilian Mountain, China

Yanyan Lv <sup>1,2</sup>, Jianguo Zhang <sup>1,2</sup>, Wei Chen <sup>1,2</sup>, Yi Sun <sup>1,2</sup>, Meng Li <sup>1,2</sup>, Hongyan Yu <sup>3</sup>, Shuhua Yi <sup>1,2</sup> and Baoping Meng <sup>1,2,\*</sup>

<sup>1</sup> Institute of Fragile Eco-Environment, Nantong University, Nantong 226007, China

<sup>2</sup> School of Geographic Science, Nantong University, Nantong 226007, China

<sup>3</sup> Qinghai Service and Guarantee Center of Qilian Mountain National Park, Xining 810001, China

\* Correspondence: mengbp18@ntu.edu.cn

**Abstract:** *Gynaephora alpherakii* (*G. alpherakii*) is one of the dominant pests in the alpine meadow; its outbreak has substantial impacts on grass vegetation production and carrying capacity. The increasing frequency of *G. alpherakii* outbreaks will take place with global warming and human activities. Therefore, it is crucial to identify inhabitable areas to apply prevention measures efficiently and facilitate sustainable grassland management. In this study, field measurements of *G. alpherakii* (from 2010 to 2021) were used to explore the relationships between its density and environmental factors in the National Park of Qilian Mountain, China. Then, the inhabitable area was mapped. The results showed that (1) eight of the twenty-five factors studied (average and maximum value of solar radiation; minimum, standard deviation, and average value of normalized difference vegetation index (NDVI); maximum precipitation; and digital elevation model) had a greater influence on *G. alpherakii* density. (2) Among all of the estimation models, models based on the average of solar radiation, the minimum of NDVI, and the maximum precipitation were better than other factors, with a higher determination coefficient ( $R^2$ ) of 0.53–0.66 and a lower root mean square error (RMSE) of 40.54–47.32 head/m<sup>2</sup>. Models based on rest factors had a lower accuracy, with  $R^2$  within 0.38–0.49 and an RMSE of 50.91–58.68 head/m<sup>2</sup>. (3) The inhabitable area which was most suited for *G. alpherakii* growth, development, and frequent outbreaks was located in the northeast of the research area (24.72%), with inhabitable decreasing from southeast to northwest. This method is helpful for clarifying the distribution regions and occurrence dynamics of the *G. alpherakii* in the alpine meadow. The spatial distribution of *G. alpherakii* in the National Park of Qilian Mountain can also be clearly defined by using this method, which can provide data support for its prevention and control.

**Keywords:** *Gynaephora alpherakii*; inhabitable areas; environmental factors; spatial distribution



**Citation:** Lv, Y.; Zhang, J.; Chen, W.; Sun, Y.; Li, M.; Yu, H.; Yi, S.; Meng, B. Mapping of *Gynaephora alpherakii* Inhabitability Area in the National Park of Qilian Mountain, China. *Agronomy* **2023**, *13*, 594. <https://doi.org/10.3390/agronomy13020594>

Academic Editor: Camilla Dibari

Received: 3 January 2023

Revised: 10 February 2023

Accepted: 16 February 2023

Published: 18 February 2023



**Copyright:** © 2023 by the authors. Licensee MDPI, Basel, Switzerland. This article is an open access article distributed under the terms and conditions of the Creative Commons Attribution (CC BY) license (<https://creativecommons.org/licenses/by/4.0/>).

## 1. Introduction

Grassland is a major part of the global terrestrial ecosystem that accounts for nearly 40% of Earth's terrestrial area, and plays a key role in regulating climate change by balancing greenhouse gases [1–3]. Alpine grassland is one of the most important grassland types, and more than 48% is distributed on the Qinghai–Tibetan Plateau (QTP) [4]. The outbreaks of rodents and insects, as well as snow and drought, are the main natural disasters in QTP [5], which pose a great threat to the grassland carrying capacity and husbandry [6]. The grassland caterpillar, pika (*Ochotona curzoniae*), zokor (*Myospalax baileyi*), and locust are the major driving forces for the degradation in grassland. For example, in the Source Region of the Yellow River (lies in the northeast of the QTP, with an area of  $1.2 \times 10^5$  km<sup>2</sup>), the damaged area caused by rodents and insects is  $3.25 \times 10^4$  km<sup>2</sup>, accounting for 34.66% of the available grassland area (25.29% and 9.38% for the rodent and insect, respectively) [5]. However, studies on the behavior, influencing factors, and regular outbreaks are focused on pika, zokor, and locust [7–10]; our knowledge of grassland caterpillars is still lacking [11,12].

There are 15 species of grassland caterpillars recorded, of which eight species are distributed in alpine grassland, and all of them are endemic species of the QTP [13,14]. The *Gynaephora alpherakii* (*G. alpherakii*), also known as the red or black head caterpillar, belongs to Gynaephora, Lymantriidae, and Lepidoptera. Previous research has indicated that *G. alpherakii* was present in the alpine meadow grassland. The *G. alpherakii* had strong preferences for Poaceae and Cyperaceae plants (including *Kobresia myosuroides*, *Kobresia humilis*, *Festuca rubra*, and *Elymus nutans*) [15]. The outbreak of *G. alpherakii* can make food shortages for the livestock. The structure of the plant community has also been changed, because *G. alpherakii* ingests the young plant branches and leaves first, which affects the grass' flowering period and development, resulting in a rise in noxious weeds and the grassland degradation intensifying [16]. Moreover, *G. alpherakii* is high in toxins, and is poisonous to livestock and humans via grazing and touching the skin [17].

The *G. alpherakii* is widely distributed on the QTP (more than 2 million hectares) with high density (usually 200–500 head/m<sup>2</sup>, the highest density reaching 3000 head/m<sup>2</sup>) [18]. Since the 1960s, tremendous efforts, time, and cost have been invested in its prevention, particularly in the study and production of chemical and biological insecticides [19,20]. However, this has still failed to mitigate the harm fundamentally and effectively. With global climate change and human activities, the frequent outbreaks of *G. alpherakii* in recent years have been recorded and have seriously harmed the animal husbandry on the QTP. Therefore, it is crucial to identify inhabitable areas to prevent *G. alpherakii* outbreaks and take measures accordingly.

The division of the inhabitable areas has been used for predicting the outbreak of the pika [21] and locust [22]. The spatial distribution can be clearly defined using this method, which can provide the data support and the decision basis for its control. However, the inhabitable area of *G. alpherakii* has still been unknown. This study aimed to investigate the influencing factors and inhabitable area of *G. alpherakii* in the National Park of Qilian Mountain. We provide a database for the forecasting, warning, and prevention of *G. alpherakii*, and it is hoped that this study will be helpful for the restoration and management of degraded grassland.

## 2. Data and Methods

### 2.1. Study Area

The study area (36.8926°–39.2110° N; 96.1380°–102.6405° E) is located in the National Park of Qilian Mountain, including Delingha City, Tianjun County, Qilian County, Gangcha County, and Menyuan County of Qinghai Province. Grassland is the most important land use type, accounting for 90% of the whole study area. The grassland types mainly include alpine meadow, mountain meadow, lowland meadow, temperate steppe, alpine steppe, alpine desert steppe, temperate desert, and alpine desert (Figure 1). The average annual precipitation is 232.4 mm, which has increased from northwest to southeast, and the higher precipitation was distributed in the central and eastern regions of the study area [23]. The mean annual temperature is 4 °C, and the spatial distribution form is relatively stable with little inter-annual variation. The temperature contour is consistent with the terrain profile [24]. The average elevation is 4000 m (Figure 1). It is an important ecological security barrier in western China, and it is also an important water source of the Yellow River and a priority area for biodiversity conservation.

### 2.2. Field Observation

The field survey plots were established throughout the study area, according to grassland type, terrain conditions, and the distribution of *G. alpherakii*, and a total of 125 plots were established during the grassland growth season (June to July) from 2010 to 2021 (Figure 1). Field survey plots were chosen to ensure a 5 km horizontal distance between plots and homogeneity of both vegetation and land use, and the geographical locations of the plots were selected to ensure that similar grassland types and geomorphology existed within a 250 m range around the plots, considering that moderate resolution imaging

spectroradiometer (MODIS) pixels are  $250\text{ m} \times 250\text{ m}$  in size. In each sample plot, three to five quadrats with an area of  $1\text{ m} \times 1\text{ m}$  were randomly set up for ground observation. The sampling record in each quadrat included latitude, longitude, elevation, grassland types, and density of *G. alpherakii* (Figure 2). Previous field investigations and research have indicated that *G. alpherakii* is mainly distributed in alpine meadow grassland. Hence, the field observation was performed in the alpine meadow grassland of the National Park of Qilian Mountain.

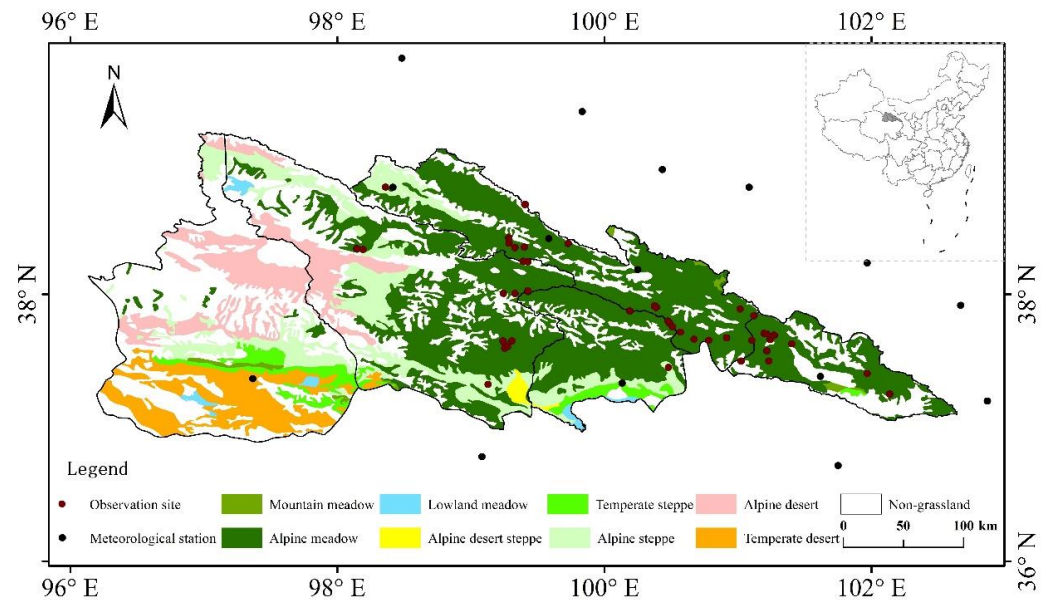


**Figure 1.** Location, grassland types, and field observations of the study area.

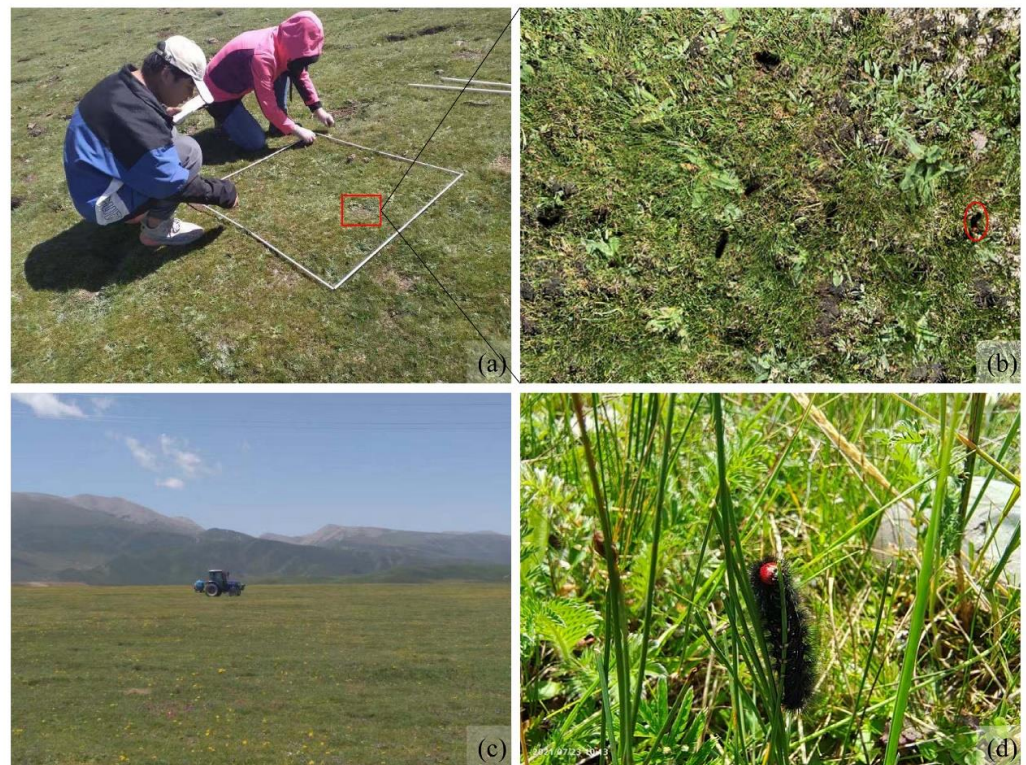


**Figure 2.** Field observation: (a) is field observation with  $1\text{ m} \times 1\text{ m}$  quadrat, (b) is the enlargement of a small part of the quadrat, (c) is the machine for spraying the chemical and biological insecticides, and (d) are the *Gynaephora alpherakii* feeding on grass.

### 2.3. Remote Sensing and Environmental Data Preprocess

NDVI data were selected from MODIS 16 d maximum value synthesis vegetation index product MOD13Q1, and the data were downloaded from the United States Geological Survey (USGS; <https://e4ftl01.cr.usgs.gov/> (accessed on 31 December 2021)). The images from May to September in 2000–2021, with a spatial resolution of 250 m (h25v05 and h26v05), were selected. Then, the ArcGIS Raster Calculator tool was used to transfer and reprocess the formation and the projection. The maximum (NDVImax), minimum (NDVImin), medium (NDVImed), average (NDVIave), range (NDVIrange), standard deviation (NDVIstd), and sum (NDVIsun) of MODIS NDVI vegetation index were calculated during the annual growing season (May to September) from 2010 to 2021.

Other environmental factors included grassland types, meteorology (temperature, precipitation, and solar radiation), soil (soil type, soil sand, and clay content) and topography (DEM) (Figure 3). The daily temperature, precipitation, and solar data used in this study were obtained from 23 official meteorological stations in the National Park of Qilian Mountain and surrounding areas, and covered the period from 2000 to 2021 (Figure 1). The growing season (May to September) data were calculated for each station. Meteorological data from outside stations were acquired using thin-plate smoothing spline (ANUSPLIN) interpolation. The data mainly include the temperature, precipitation, and solar radiation from 2000–2021 with a spatial resolution of 5 km. Maximum, minimum, average, and sum values of temperature (TEMmax, TEMmin, TEMave, and TEMsum), precipitation (PREmax, PREmin, PREave, and PREsum), and solar radiation (SRAmx, SRAmn, SRAave, and SRAsum) in the growing season (May to September) from 2011 to 2021 were calculated using the ArcGIS Raster Calculator (Figure 3). The soil type data were downloaded from the vectorized dataset 1:1,000,000 Soil Map of the People’s Republic of China, compiled and published by the National Soil Census Office in 1995 (<https://www.resdc.cn/data> (accessed on 20 December 2021)). Grassland-type data were collected using the 1:100,000 China Grassland Resource map (1:100,000 China Grassland Resource Atlas, 1993) [25]. Soil clay and sand content data were downloaded from the northwest ecological environment resources of the Chinese Academy of Sciences Institute of Cold and Arid Regions of the Science Data Center (<http://westdc.westgis.ac.cn/data/> (accessed on 12 December 2020)). Terrain data were obtained from the spatial information alliance website (<http://srtm.csi.cgiar.org/> (accessed on 12 December 2020)).

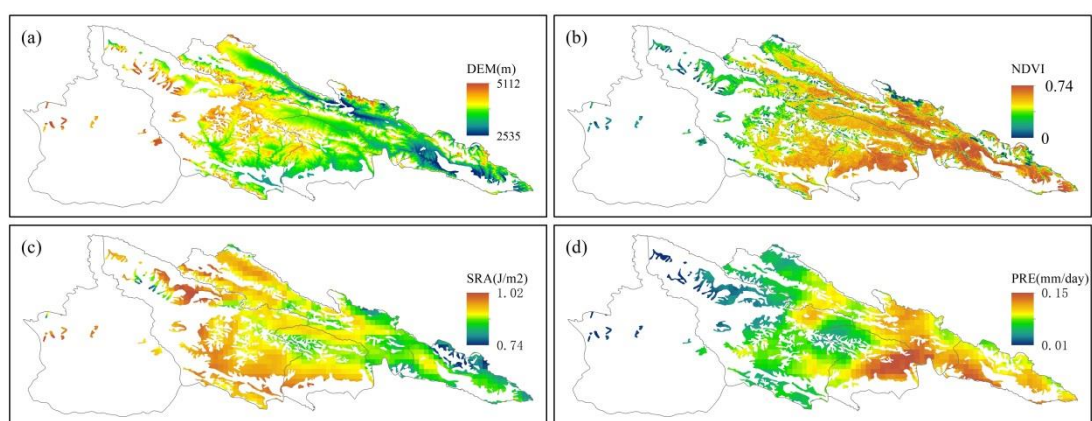


**Figure 3.** Spatial distribution of (a) digital elevation model (DEM); (b) average value of normalized difference vegetation index (NDVI) from 2000 to 2021; (c) average value of solar radiation (SRA) from 2000 to 2021; and (d) average value of precipitation (PRE) from 2000 to 2021.

The above data were uniformly transformed into Albers in ArcGIS software, and resampled into raster images with a resolution of 250 m (each raster datum has the same number of rows and columns), so as to be used as an input in the later construction and prediction of *G. alpherakii*.

## 2.4. The Inhabitable Index of Each Variable

### 2.4.1. Environmental Factors Selection

In order to reduce the influence of the autocorrelation and information redundancy among the environmental factors, the Pearson coefficients, calculated using the R package “rcorr”, were used to screen factors first, and only one factor was retained if  $|r| > 0.7$  between two factors. Then, the boosted regression tree (BRT) analysis [26,27], created using the R packages “gbm” [28,29] and “dismo” [30], was used to examine the relationship between potential predictors and environmental factors. Additionally, the relative contribution (RC) was used to assess the relevance of each factor in BRT models [31]. This metric measures how often the predictor was selected for partitioning, weighted by the squared model improvement resulting from successive partitions [32]. Finally, cumulative RC factors greater than 85% were retained for further analysis.

### 2.4.2. Division of the Inhabitable Index of *G. alpherakii*

The average density in all quadrats of each plot was estimated as the *G. alpherakii* density for that observation plot. The *G. alpherakii* density of different sample plots was taken as the dependent variable and environmental factors (selected via autocorrelation and BRT) were taken as the independent variables. The polynomial models were employed for calculating their correlations with *G. alpherakii* density in this study [33,34]. Additionally, the leave-one-out cross validation (LOOCV) method, root mean square error (RMSE), and determination coefficient ( $R^2$ ) were used to evaluate the accuracy of the regression models [35].

Combing the density estimation models and grassland damage caused by *G. alpherakii*, each factor’s inhabitable index (IH) was divided into five classes (Table 1). When the inhabitable index was 1, it had the main conditions for the growth and development of pests, and it showed a potentially harmful area for pests. However, when the inhabitable index was 5, it was very suitable for the growth and development of pests and grassland was often damaged by pests.

**Table 1.** Inhabitable index of *Gynaephora alpherakii*.

Inhabitable Index	Degree of Damage	Degree of Inhabitation	Density (Head/m <sup>2</sup> )
1	No damage	Potential area	0–30
2	Mild	Suitable	31–80
3	Moderate	More suitable	81–130
4	Severe	Very suitable	131–180
5	Serious	Extremely suitable	181–230

Note: derived from prevention and treatment measures of pika and insects in the grassland of Qinghai Province.

### 2.5. Division of the Inhabitable Area of *G. alpherakii*

The IH distribution patterns were mapped based on *G. alpherakii* density estimation models and Table 1; the inhabitable area was calculated by the weight of each selected factor (calculated in Section 2.4.1) and Equation (1).

$$IH(x, y) = \sum_{i=1}^n E_i(x, y)W_i \quad (1)$$

where  $IH(x, y)$  represented the pixel inhabitable index with coordinate  $(x, y)$ ;  $n$  represented the number of environmental factors;  $E_i(x, y)$  represented the pixel value of  $i$ -th factor in coordinate  $(x, y)$ ;  $W_i$  represented the weight of  $i$ -th factor;  $W_i$  was calculated by the boosted regression tree algorithm in Section 2.4.1; and  $i = 1, 2, 3, \dots, n$ .

Finally, the inhabitable areas were mapped based on Table 2.

**Table 2.** Inhabitable areas of *Gynaephora alpherakii*.

Inhabitable Area	Classification Standard	Description
1	$4 \leq IH$	It is very suitable for the growth and development of <i>G. alpherakii</i> and is often damaged by <i>G. alpherakii</i> .
2	$3 \leq IH < 4$	It is more suitable for the growth and development of <i>G. alpherakii</i> , and it is the area that <i>G. alpherakii</i> often harms.
3	$2 \leq IH < 3$	It is suitable for the growth and development of <i>G. alpherakii</i> , and is sometimes harmed by <i>G. alpherakii</i> .
4	$IH \leq 2$	It has the main conditions for the growth and development of <i>G. alpherakii</i> , and is the potential harm area of <i>G. alpherakii</i> .

Note: IH represented the inhabitable index.

### 3. Results

#### 3.1. The Autocorrelation and Boosted Regression Tree Analysis of Environmental Factors

The results of the autocorrelation analysis are shown in Figure 4; according to the Pearson coefficient between any two factors, a total of twelve factors were selected for further boosted regression tree analysis (including NDVIave, NDVImin, NDVIstd, PREave, PREmax, SRAave, SRAmax, Clay 1 (clay concentration of surface soil), Clay 2 (clay concentration of bottom soil), Sand 2 (the sand concentration of bottom soil), soil type, and DEM). The Pearson coefficient was higher than 0.7, and each of the correlations is shown in the Supplementary Figures (Figures S1–S3).

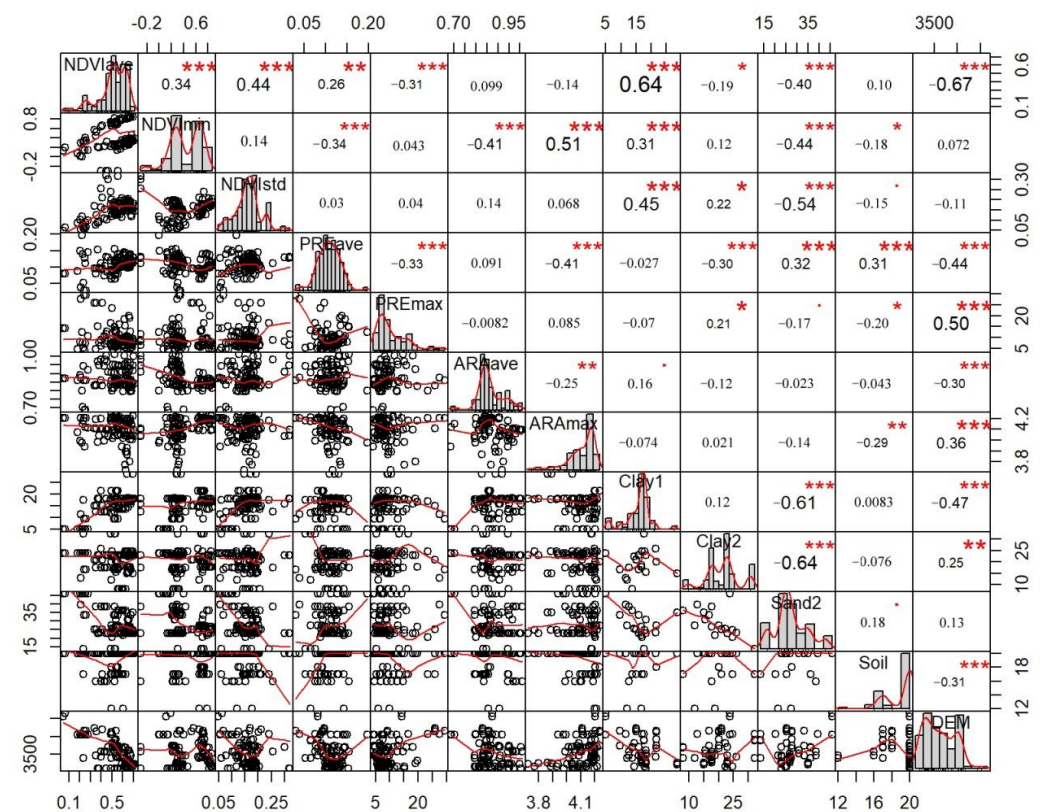


**Figure 4.** The correlation of Pearson coefficient among factors. NDVIave, NDVImin, NDVIstd, PREave, PREmax, SRAave, SRAmax, Clay 1, Clay 2, Sand 2, Soil, and DEM refer to average NDVI, minimum NDVI, standard deviation of NDVI, average precipitation, maximum precipitation, average solar radiation, maximum solar radiation, clay concentration of surface/bottom soil, sand concentration of bottom soil, soil type, and digital elevation mode, respectively. \* denotes  $p < 0.05$ ; \*\* denotes  $p < 0.01$ ; \*\*\* denotes  $p < 0.001$ .

The relative contribution of each environmental factor is exhibited in Figure 5. SRAave and NDVImin had relative contribution values higher than 10%. The total contribution reached 36.17% (22.6% and 13.5% for the SRAave and NDVImin, respectively). There were seven parameters with a relative contribution of 5% to 10%, including PREmax, NDVIstd, Sand 2, DEM, SRAMax, NDVIave, and PREave. The relative contribution values for the other components, which mostly included soil type, Clay 1, and Clay 2, were lower than 5%. The overall contribution of the first eight components approached 85% among all indices.

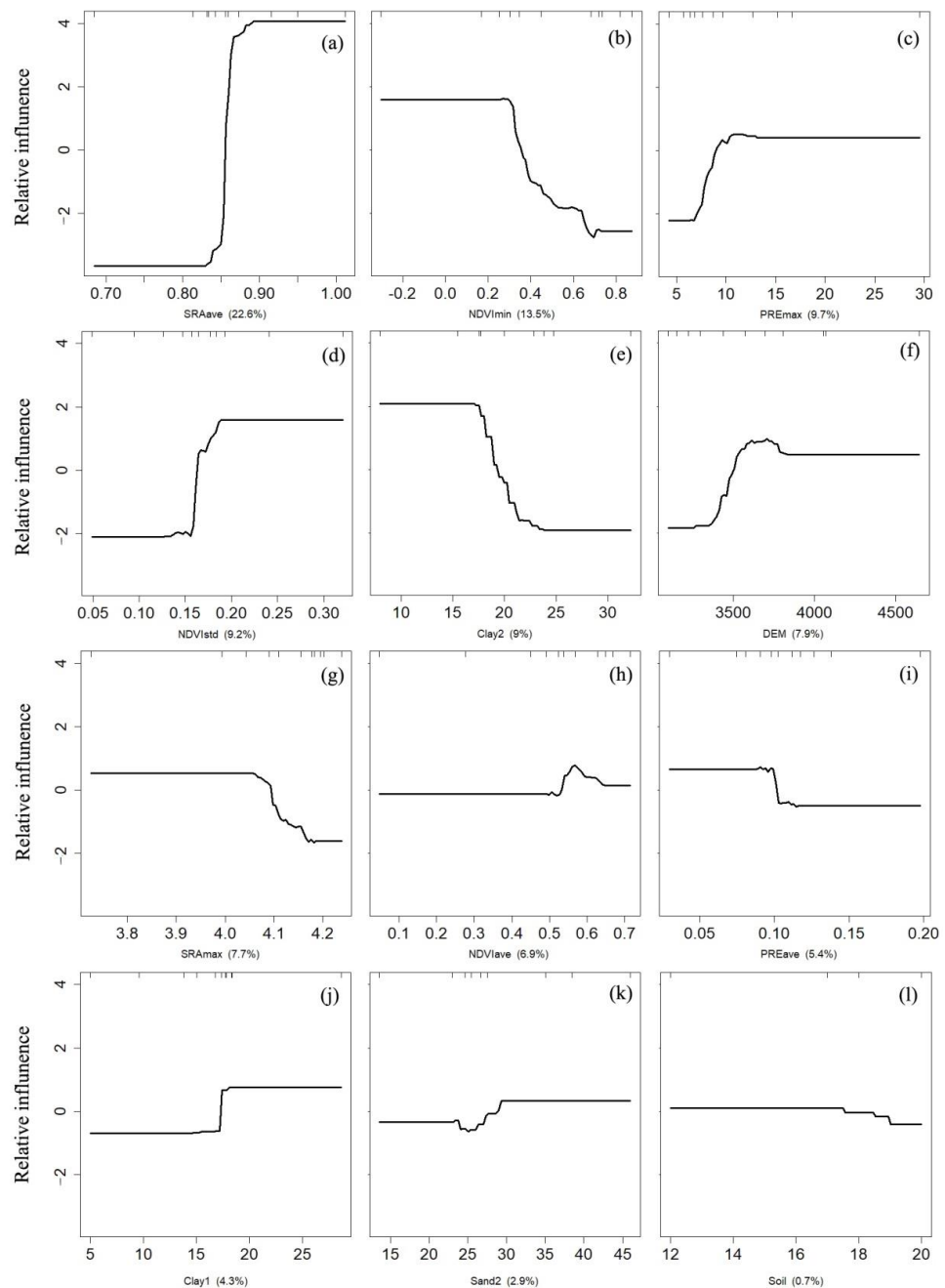


**Figure 5.** Relative contribution of each factor from 2000 to 2021: (a–l) refers to the average solar radiation (SRAave), minimum NDVI (NDVImin), maximum precipitation (PREmax), standard deviation of NDVI (NDVIstd), clay concentration of bottom soil (Clay 2), digital elevation model (DEM), maximum solar radiation (SRAMax), average NDVI (NDVIave), average precipitation (PREave), clay concentration of bottom soil (Clay 1), sand concentration of bottom soil (Sand 2), and soil type (Soil), respectively. X is the value of each environmental factor.

### 3.2. Relationship between Environmental Factors and *G. alpherakii* Density

The polynomial models were used to develop the estimating model in conjunction with the environmental parameters (filtered in Section 3.1) and the observed *G. alpherakii* density. Figure 6 and Table 3 depict the estimation models and the accuracy examination. Among all estimating models, models based on SRAave, NDVImin, and PREmax performed better than others, with a higher R<sup>2</sup> within 0.53–0.66 and a lower RMSE of 40.54–47.32 head/m<sup>2</sup>. While Clay 2 models are the most accurate, SRAMax and NDVIave come in second, with R<sup>2</sup> within 0.41–0.49 and an RMSE of 50.91–58.68 head/m<sup>2</sup>. The accuracy of the model based on NDVIstd is worse, with an R<sup>2</sup> of 0.38 and a greater RMSE of 55.29 head/m<sup>2</sup>, respectively.

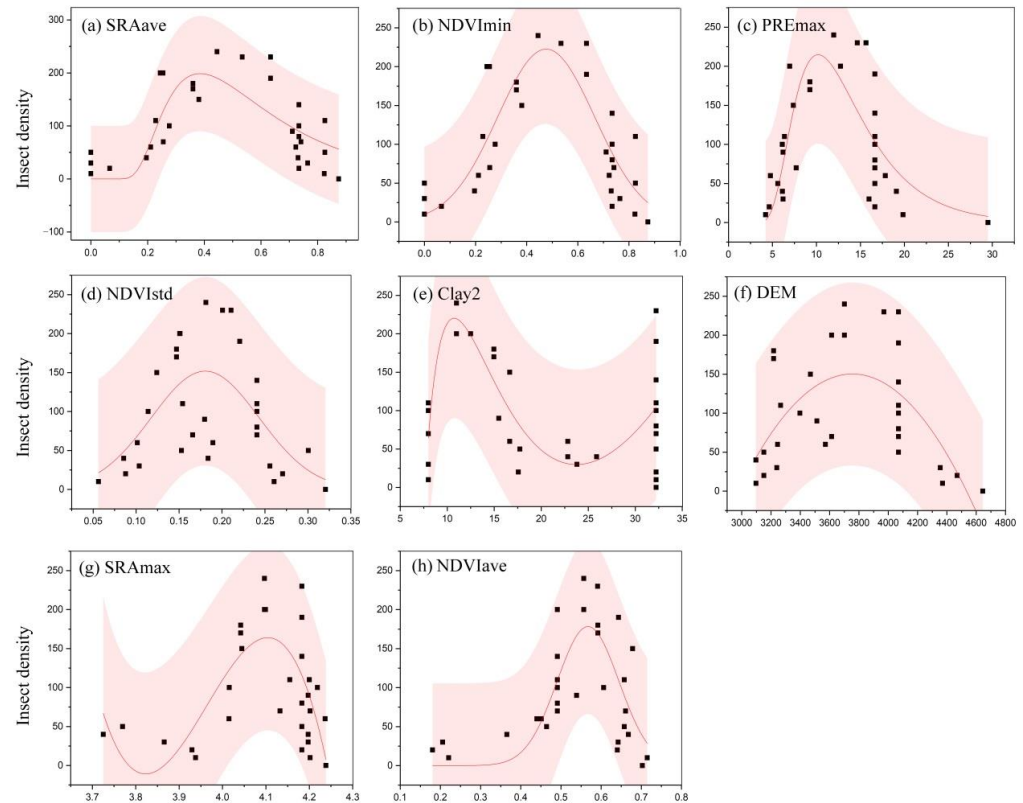


**Figure 6.** Relationship between environmental factors and *Gynaephora alpheraki* density: (a–h) refer to the average solar radiation (SRAave), minimum NDVI (NDVImin), maximum precipitation (PREmax), standard deviation of NDVI (NDVIstd), clay concentration of bottom soil (Clay 2), digital elevation model (DEM), maximum solar radiation (SRAMax), and average NDVI (NDVIave), respectively. The dash area presents a 95% confidence interval.

**Table 3.** Fitted models based on SRAave, NDVImin, PREmax, NDVIstd, Clay 2, DEM, SRAMax, and NDVIave.

Factors	Models	R <sup>2</sup>	RMSE (Head/m <sup>2</sup> )
SRAave	$y = \text{Exp}(7.47618 - 3.7811x - 0.108/x^2)$	0.54 **	45.57
NDVImin	$y = \text{Exp}(2.27319 + 13.15692x - 13.81686x^2)$	0.66 **	40.54
PREmax	$y = \text{Exp}(8.78282 - 0.22318x - 118.28301/x^2)$	0.53 **	47.32
NDVIstd	$y = 0.89164 + 45.77443x - 126.80326x^2$	0.38 *	55.29
Clay 2	$y = -2405.81133 + 44.04946x + 41153.48634/x - 193652.51082/x^2$	0.41 *	53.18
DEM	$y = -3345.77169x - 2.47865 \times 10 - 4x^2$	0.41 *	53.37
SRAMax	$y = 972994.0304 - 738248.15298x + 186490.90176x^2 - 15683.83293x^3$	0.42 *	58.68
NDVIave	$y = \text{Exp}(-21.99 + 95.78044x - 84.40237x^2)$	0.49 **	50.91

Note: R<sup>2</sup> and RMSE refer to the determination coefficient and root mean square error, respectively. SRAave, NDVImin, PREmax, NDVIstd, Clay 2, DEM, SRAMax, and NDVIave refer to the average solar radiation, minimum NDVI, maximum precipitation, standard deviation of NDVI, clay concentration of bottom soil, DEM, maximum solar radiation, and average NDVI, respectively. \* and \*\* denote  $p < 0.05$  and  $p < 0.01$ , respectively.

### 3.3. Spatial Variation in the Inhabitable Index for Different Factors

The distribution of the inhabitable index (IH) for each variable was mapped using estimating models based on chosen factors (Figure 7) and the rule of the IH division (Table 1). The IH of SRAave, NDVimin, PREmax, NDVlst, DEM, and NDVIave all revealed a similar variation pattern, decreasing from southeast to northwest of the research region. Nevertheless, the IH of Clay 2 and SRMax exhibited a contrasting variance pattern, increasing from the southeast to the northwest of the research region. The IH value of 4 had the highest area percentage in NDVlst, DEM, and SRMax, accounting for 40%, 53%, and 51% of the study area, respectively. The factors of SRAave, Clay 2, and NDVIave had a higher proportion in IH 3, IH 2, and IH 1, respectively. For PREmax, the majority of the region falls within the IH of 5, accounting for 87% of the research area.

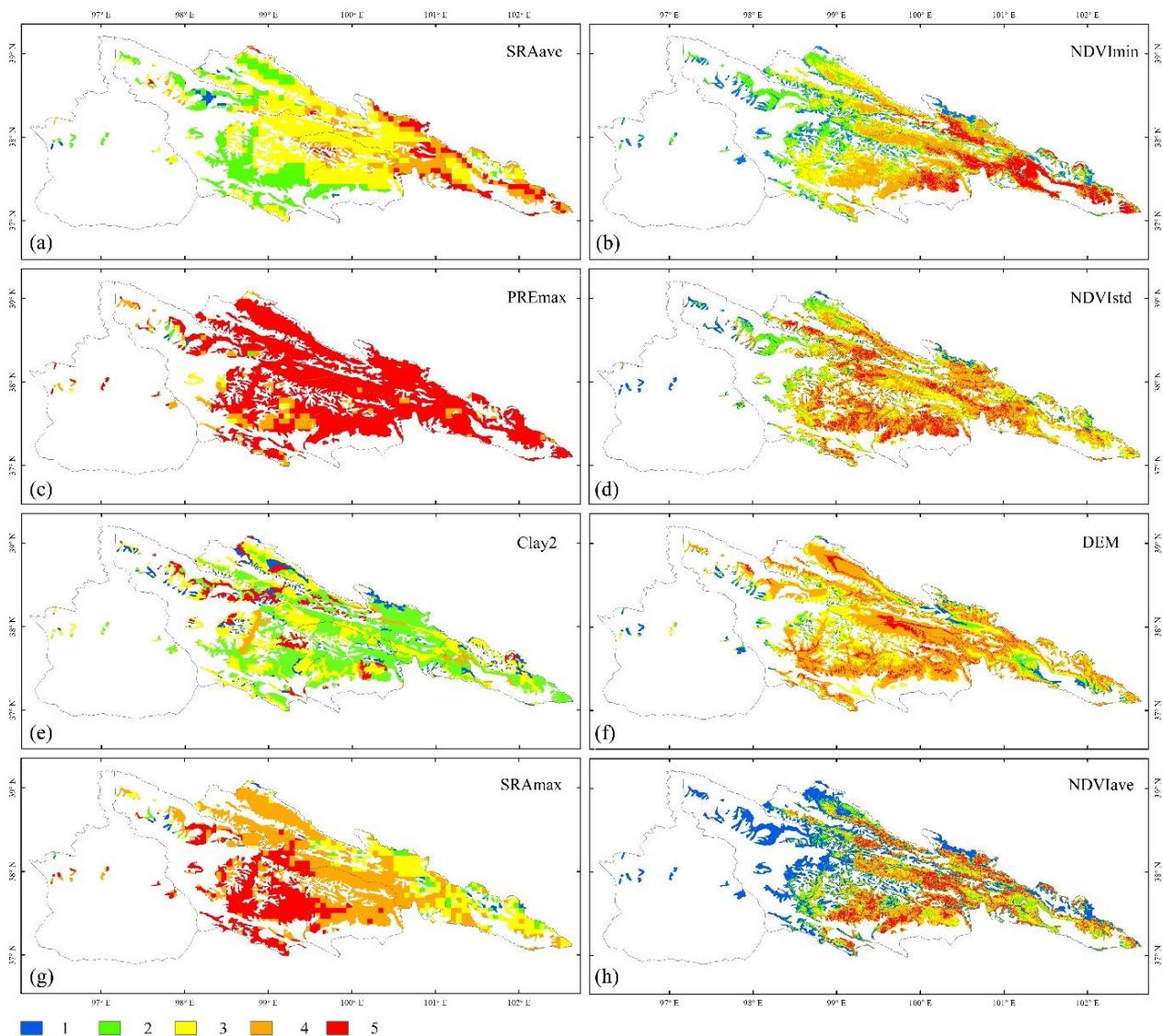


**Figure 7.** Spatial variation in the inhabitable index for different factors: 1–5 represent the inhabitable index; the degree of damage ranged from no damage to mild, moderate, severe, and serious, respectively. (a–h) refer to the average solar radiation (SRAave), minimum NDVI (NDVimin), maximum precipitation (PREmax), standard deviation of NDVI (NDVlst), clay concentration of bottom soil (Clay 2), digital elevation model (DEM), maximum solar radiation (SRMax), and average NDVI (NDVIave), respectively.

### 3.4. Classification of Inhabitable Area

The inhabitable area referred to the area suited for the growth and development of *G. alpherakii*. In this study, Inhabitable Area 1 was very suitable for the growth and development of pests and was often damaged by *G. alpherakii*, and the inhabitability was decreased to Inhabitable 4. As shown in Figure 8, the Inhabitable Areas 1 and 2 were mostly dispersed in the northeast of the research region, accounting for 24.72% and 37.88% of the study area, respectively. The Inhabitable Areas 3 and 4 were mostly distributed in the north and west of the research region. The area of Inhabitable Area 3 accounted for 30.09% of the whole research area, while the area of Inhabitable Area 4 was the smallest, accounting for 7.30% of the total study area.

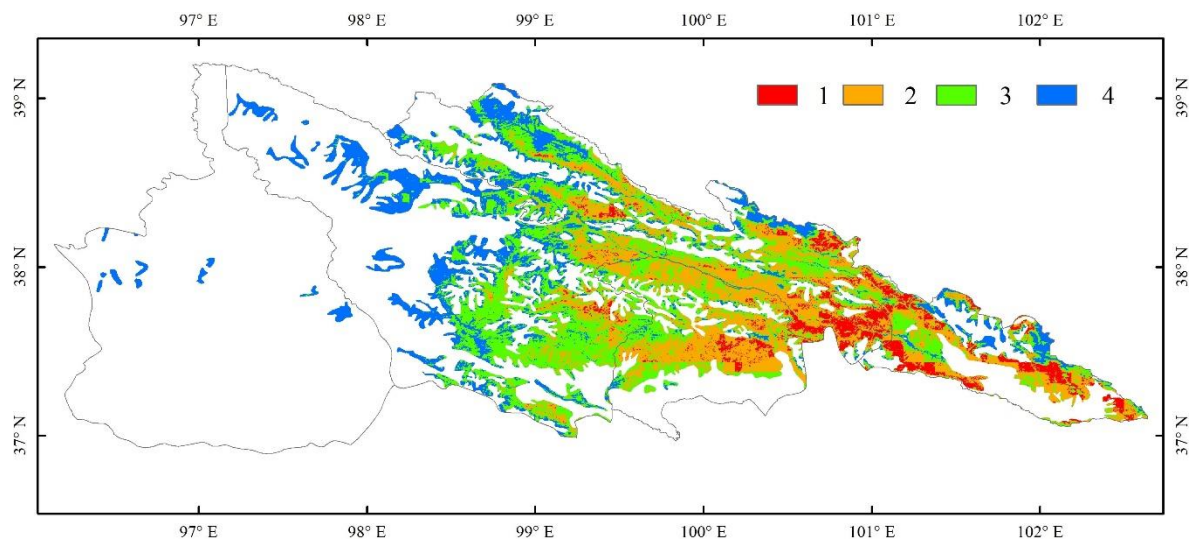


**Figure 8.** Spatial distribution of *Gynaephora alpherakii* inhabitable area; note: Inhabitable Areas 1–4 mean the inhabitability was very suitable, more suitable, suitable, and potentially suitable for the growth and development of pests, respectively.

## 4. Discussion

### 4.1. Implications of *G. alpherakii*'s Inhabitable Area

The *G. alpherakii* was widely distributed in the alpine meadow grassland and its outbreak severely destroyed the grassland vegetation [36]. As a result, the grassland productivity and carrying capacity were significantly jeopardized. The preventative measures were implemented following *G. alpherakii* outbreaks (usually distinguished by *G. alpherakii* density). The limitations are clear: (1) existing preventions were mainly conducted after the *G. alpherakii* outbreak, and early prediction and warning were inadequate [37]. There was still a challenge to organize the labors and chemical insecticides immediately in the widely distributed pasture area. (2) The *G. alpherakii* was mainly prevented through spraying the chemical insecticides manually or mechanically, which could be easily affected by the climate conditions (such as wind and rain), leading to poor efficiency or outbreaks again; (3) although the excessive chemical insecticides effectively prevented the outbreak of *G. alpherakii*, the pollution to grass vegetation (pesticides affect grasslands by affecting soil fauna and microbial organisms) and soil was increased, which destroyed the biodiversity in the original habitat and caused a huge threat to the ecological environment [38]. Therefore, early warning prediction before its outbreak was a vital strategy for *G. alpherakii* prevention.

As we know, the inhabitable area referred to the areas suited for the establishment and development of grassland biology, and it provided early warning signals [39]. In this study, *G. alpherakii*'s inhabitable area was explored based on its density and environmental conditions. The most favorable areas for *G. alpherakii* outbreak and development lied in the northeast (Inhabitable Area 1, with an area proportion of 24.72%), and the inhabitability declined from southeast to northwest (Figure 8). As a result, Inhabitable Area 1 needs to

enhance management. On the contrary, labor and costs should be reduced to the northwest of the research area (Inhabitable Area 4, with an area percentage of 7.3%).

#### 4.2. Environmental Factors and Influence

Because *G. alpherakii* outbreaks were caused by specific environmental circumstances, understanding their biological properties, outbreak regularity, quantitative fluctuation, and major influencing factors was critical for forecasting, warning, and prevention. In our study, the SRAve had the most effect in this research, with a relative value of 22.6% (Figure 5). This may be connected to their preferences for warm, sunny climates, especially as the larvae enter a stage of rapid growth and the solar radiation was required to sustain themselves for the growth requirements [40,41]. The NDVI has a high-value relative effect (NDVImin, NDVIstd, and NDVIave were 13.5%, 9.2%, and 6.9%, respectively) (Figure 5). This phenomenon can be explained in that grassland flora in alpine meadows was a significant influence parameter on *G. alpherakii* food limitation. The *G. alpherakii* favored the Kobresia species, which were the dominating plants in the alpine meadow. Wang and Liu (2022) used a random sample approach to evaluate the density and its relationships with vegetation in 10 plots and discovered a negative association between both [42]. However, Yu and Shi (2010) discovered that whereas aboveground biomass has a substantial positive association with density, subsurface biomass and the grassland vegetation height have a non-significant link with total vegetation coverage [43]. When the density reaches a severe level, the grassland vegetation cover may decline drastically.

The DEM also has a strong relative correlation; the altitude influences the distribution of the *G. alpherakii*. According to studies, the majority of *G. alpherakii* is found above 4000 m [13,36]. The adaptation to this severe environment may be connected to its own genetic mechanism [14,36] and can change its fundamental metabolism to compensate for the low oxygen pressure [21]. Due to the high auto-correlation between the DEM and temperature, the relative correlation between the temperature and *G. alpherakii* density has not been investigated in our study. However, temperature is also an essential component. *G. alpherakii* showed high adaptability to the extremely cold ecological environment during its evolution [44]. The optimum temperature for *G. alpherakii* growth was 20 °C [45].

In this study, both SRA, NDVI, and DEM were crucial to *G. alpherakii* with a relative effect of more than 50% (Figure 5). The optimum SRA, NDVI, and DEM ranged from 0.80 J/h.m<sup>2</sup> to 0.89 J/h.m<sup>2</sup>, 0.54 to 0.63, and 3470 m to 4040 m, respectively. Additionally, these were mainly located in the northeastern part of the study area. On the contrary, the SRA and DEM were higher than 0.89 J/h.m<sup>2</sup> and 4040 m, and NDVI was lower than 0.54.

#### 4.3. Limitations and Prospects of *G. alpherakii* Monitoring

This study investigated the inhabitable area of *G. alpherakii* and provided a basis for its control; nevertheless, there are certain limitations: (1) With the exception of MODIS remote sensing and topography data, the other dataset was primarily interpolated by limited observations and coarse spatial resolution. The classification of *G. alpherakii*'s inhabitable area still has some errors and uncertainties. The higher resolution of the climate dataset, derived by remote sensing, should be considered to reduce the errors and uncertainties in future work. (2) The density of *G. alpherakii* was the foundation for classifying the inhabitable area. In our study, the data were mostly gathered through field observation using traditional methods, which were time-consuming, labor-intensive, and expensive. It was still a challenge to carry out large-scale survey work in a restricted period, since most of the *G. alpherakii* were distributed in a harsh environment [13], making it difficult to carry out the field research work. (3) There were no regular observation locations, and the measuring standards were not uniform [37]. The data collected by various approaches vary greatly, and there are significant uncertainties in acquiring field observations in large-scale locations. Although the remote sensing satellite can acquire large-scale data, limited by the resolution it cannot be applied in *G. alpherakii* monitoring. Therefore, new methods should be developed to acquire fixed, repeated, large-area, and longtime data.

Recently, small unmanned aerial vehicle (UAV) technology has been used in *G. alpherakii* monitoring [46]. The Mavic 2 UAV has a resolution of 0.09 cm, which ensures the identification of *G. alpherakii* from an aerial photograph [47]. Furthermore, the development of the FragMap system realized long-term, repeated, and large-scale monitoring [48], which had easy operation and was time-saving (Figure S4. Unmanned aerial vehicle field observation). The aerial photograph can provide primary data for the *G. alpherakii* field observation on a large scale, and enables the inhabitable area to be more accurate [49]. However, *G. alpherakii* is currently recognized artificially from the photograph and it is still time-consuming. Therefore, automatic image recognition should be developed in further studies.

## 5. Conclusions

Based on field observation and multi-source environmental factors, this study explored the relationship between *G. alpherakii* density and the main influencing factors. Our results showed that the average and maximum of solar radiation, minimum, standard deviation, and average of NDVI, maximum of precipitation, and DEM are the main influencing factors of *G. alpherakii* inhabitability. The polynomial models can estimate the *G. alpherakii* density effectively. The inhabitable area most suitable for *G. alpherakii* growth, development, and outbreak lies in the northeast of the study area (24.72%), and inhabitability decreased from northwest to southeast. In future work, UAV technology realizing long-term, repeated, and large-scale monitoring and automatic image recognition should be developed.

**Supplementary Materials:** The following are available online at <https://www.mdpi.com/article/10.3390/agronomy13020594/s1>. Figure S1. The auto-correlation among the NDVImax, NDVImean, NDVImedian, NDVImin, NDVIstd, NDVIsum, NDVIrange; Figure S2. The auto-correlation among the PREave, PREmax, PREsum, TMPave, TMPmax, TMPmin, TMPmin, TMPsum; Figure S3. The auto-correlation among the SRAave, SRAmax, SRAsum, Clay1, Clay2, Sand1, Sand 2, Soil, DEM; Figure S4. Unmanned aerial vehicle field observation.

**Author Contributions:** All authors contributed significantly to this manuscript. Y.L. and B.M. designed this study; Y.L., J.Z., W.C., M.L., Y.S., B.M. and H.Y. were responsible for the field observation, data processing, and analysis; Y.L. and B.M. were responsible for the writing of the paper. S.Y. made valuable revisions and conducted the editing of the paper. All authors have read and agreed to the published version of the manuscript.

**Funding:** This study was supported by the investigation and monitoring of grassland pests in the National Park of Qilian Mountain ((2021)485), and the national standardized demonstration area of green prevention and control of insect pest in grassland (SFQ11-90).

**Institutional Review Board Statement:** Not applicable.

**Informed Consent Statement:** Not applicable.

**Data Availability Statement:** NDVI data were downloaded from <https://e4ftl01.cr.usgs.gov/> (accessed on 31 December 2021); The soil type data were downloaded <https://www.resdc.cn/data> (accessed on 20 December 2021); Soil clay and sand content data were downloaded from <http://westdc.westgis.ac.cn/data/> (accessed on 12 December 2020); Terrain data were obtained from <http://srtm.csi.cgiar.org/> (accessed on 12 December 2020).

**Acknowledgments:** We thank the National Park of Qilian Mountain for providing the field observation.

**Conflicts of Interest:** The authors declare no conflict of interest.

## References

1. Loveland, T.R.; Gallant, A.L.; Vogelmann, J.E. *Perspectives on the Use of Land-Cover Data for Ecological Investigations*; Cambridge University Press: Cambridge, UK, 2005.
2. Wang, F.; Wang, S.Q.; Han, X.Z.; Wang, F.X.; Zhang, K.Q. Soil moisture dynamics of different land-cover types in the black soil regions of China. *Chin. J. Eco-Agric.* **2009**, *17*, 256–260. [[CrossRef](#)]
3. Wang, D.; Wu, G.L.; Liu, Y.; Yang, Z.; Hao, H.M. Effects of grazing exclusion on CO<sub>2</sub> fluxes in a steppe grassland on the Loess Plateau (China). *Ecol. Eng.* **2015**, *83*, 169–175. [[CrossRef](#)]

4. Lin, L.; Li, Y.K.; Xu, X.L.; Zhang, F.W.; Du, Y.G.; Liu, S.L.; Guo, X.W.; Cao, G.M. Predicting parameters of degradation succession processes of Tibetan Kobresia grasslands. *Solid Earth Discuss.* **2015**, *7*, 2185–2211. [[CrossRef](#)]
5. Wang, X.G. The current situation of rodents pests and its control methods in resource area of Huanghe River. *Qinghai Pratac.* **2000**, *3*, 19–20. (In Chinese)
6. Zhang, Q.L.; Zhang, L.; Zhao, T.X.; Wang, J.; Zhu, Q.H.; Chen, J.Y.; Yuan, M.L. Gene sequence variations and expression patterns of mitochondrial genes are associated with the adaptive evolution of two *Gynaephora* species (Lepidoptera: Lymantriinae) living in different high-elevation environments. *Gene* **2017**, *610*, 148–155. [[CrossRef](#)]
7. Qin, Y.; Huang, B.; Zhang, W.; Yu, Y.H.; Yi, S.H.; Sun, Y. Pika burrowing activity promotes vegetation species diversity in alpine grasslands on the Qinghai-Tibetan Plateau. *Glob. Ecol. Conserv.* **2021**, *31*, e01806. [[CrossRef](#)]
8. Sumbh, O.; Hof, A.R. Can pikas hold the umbrella? Understanding the current and future umbrella potential of keystone species Pika (*Ochotona* spp.). *Glob. Ecol. Conserv.* **2022**, *38*, e02247. [[CrossRef](#)]
9. Su, J.H.; Ji, W.H.; Li, H.; Yao, T.; Wang, J.F.; Nan, Z.B. Zokor disturbances indicated positive soil microbial responses with carbon cycle and mineral encrustation in alpine grassland. *Ecol. Eng.* **2020**, *144*, 105702. [[CrossRef](#)]
10. Klein, I.; van der Woude, S.; Schwarzenbacher, F.; Muratova, N.; Slagter, B.; Malakhov, D.; Oppelt, N.; Kuenzer, C. Predicting suitable breeding areas for different locust species—A multi-scale approach accounting for environmental conditions and current land cover situation. *Int. J. Appl. Earth Obs. Geoinf.* **2022**, *107*, 102672. [[CrossRef](#)]
11. Poggi, S.; Sergent, M.; Mammeri, Y.; Plantegenest, M.; Cointe, R.L.; Bourhis, Y. Dynamic role of grasslands as sources of soil-dwelling insect pests: New insights from in silico experiments for pest management strategies. *Ecol. Model.* **2021**, *440*, 109378. [[CrossRef](#)]
12. Cao, Y.; Yang, X.Z.; Zhang, L.J.; Li, M.; Yuan, M.L. Gut bacteria communities differ between *Gynaephora* species endemic to different altitudes of the Tibetan Plateau. *Sci. Total Environ.* **2021**, *777*, 146115. [[CrossRef](#)]
13. Zhang, Q.L.; Yuan, M.L. Research status and prospect of grassland caterpillars (Lepidoptera: Lymantriidae). *Pratac. Sci.* **2013**, *30*, 638–646.
14. Yu, X.C.; Chen, K.L.; Yao, B.Q.; Ma, Z.; Wang, W.Y.; Wang, H.C.; Zhao, X.; Zhou, H. Effects of simulated warming on the growth and development of *Gynaephora menyuanensis* larvae. *Acta Ecol. Sin.* **2016**, *36*, 8002–8007. [[CrossRef](#)]
15. Zheng, L.L.; Song, M.H.; Yin, T.F.; Yu, F.H. Feeding preference of *Gynaephora menyuanensis* and its relationships with plant carbon and nitrogen contents in an alpine meadow on the Tibetan plateau. *Acta Ecol. Sin.* **2016**, *36*, 2319–2326. [[CrossRef](#)]
16. Zhou, H.K.; Wang, X.H.; Wen, J.; Zhu, J.H.; Ye, X.; Wang, W.Y.; Chen, Z. The relationship between damage of grassland caterpillar and climate factors in the Maqin County of Guoluo Prefecture. *Pratac. Sci.* **2012**, *29*, 128–134. [[CrossRef](#)]
17. Liu, W.Q.; He, D.S.; Ni, M. The harm of stomatitis caused by grassland caterpillar in grazing livestock. *Pratac. Ani. Hus.* **2011**, *3*, 58–61.
18. Yang, F. Comparative research on effect of nine insecticides for grassland caterpillar indoor. *Chin. Qinghai J. Anim. Vet. Sci.* **2005**, *35*, 5–7. [[CrossRef](#)]
19. Liu, S.G.; Yang, R.Z.; Wu, T.Q. Development and application of insecticide for grassland caterpillar Virus. *J. Grass Ind.* **1993**, *2*, 47–50.
20. Zhang, J.J.; Zhou, C.G.; Guo, G.Z.; Zhang, Y.M. Research progress in the synergy of the baculovirus insecticides. *J. Shandong Agric. Univ. Nat. Sci.* **2003**, *35*, 154–158. [[CrossRef](#)]
21. Zhao, D.J.; Zhang, Z.Y.; Cease, A.; Harrison, J.; Kang, L. Efficient utilization of aerobic metabolism helps Tibetan locusts conquer hypoxia. *BMC Genom.* **2013**, *14*, 631. [[CrossRef](#)]
22. Zhao, L.L.; Huang, W.J.; Chen, J.S.; Dong, Y.Y.; Ren, B.Y.; Geng, Y. Land use/cover changes in the Oriental migratory locust area of China: Implications for ecological control and monitoring of locust area. *Ecosyst. Environ.* **2020**, *303*, 107110. [[CrossRef](#)]
23. Huang, Y.; Mao, W.Q.; Wang, X.Y. Temporal and spatial distribution of precipitation in the Qilian Mountain and its surrounding areas in recent 39 Years. *Meteorol. Drought* **2020**, *38*, 527–534. [[CrossRef](#)]
24. Zhang, C.J.; Guo, N. Climatic variation characteristics over Qilian Mountain area during the last 40 Years. *Meteorol. Mon.* **2002**, *28*, 33–39. [[CrossRef](#)]
25. 1 million China Grassland Resource Map Compilation Committee. *1:1 Million China Grassland Resource Atlas*; China Cartographic Publishing House: Beijing, China, 1993.
26. Hiwat, H.; Bretas, G. Ecology of anopheles darlingi root with respect to vector importance: A review. *Parasites Vectors* **2011**, *4*, 177. [[CrossRef](#)]
27. Gareth, J.; Daniela, W.; Trevor, H.; Robert, T. *An Introduction to Statistical Learning with Applications in R*; Computing Reviews; Springer: Berlin/Heidelberg, Germany, 2014.
28. Greg, R. *gbm: Generalized Boosted Regression Models. R package version 2.1.5*; 2004. Available online: <http://cran.ma.imperial.ac.uk/web/packages/gbm/> (accessed on 15 February 2022).
29. Hijmans, R.J.; Phillips, S.; Leathwick, J.R.; Elith, J. *Dismo package for R, version 1.1–4*; 2017; Available online: <https://cran.r-project.org/web/packages/dismo/dismo.pdf> (accessed on 15 February 2022).
30. Elith, J.; Leathwick, J.R.; Hastie, T. A working guide to boosted regression trees. *J. Anim. Ecol.* **2008**, *77*, 802–813.
31. Rodríguez, L.; García, J.J.; Carreño, F.; Martínez, B. Integration of physiological knowledge into hybrid species distribution modelling to improve forecast of distributional shifts of tropical corals. *Divers. Distrib.* **2019**, *25*, 715–728. [[CrossRef](#)]

32. Brock, P.M.; Fornace, K.M.; Grigg, M.J.; Anstey, N.M.; William, T.; Cox, J.; Drakeley, C.J.; Ferguson, H.M.; Kao, R.R. Predictive analysis across spatial scales links zoonotic malaria to deforestation. *Proc. Biol. Sci.* **2019**, *286*, 20182351. [[CrossRef](#)]
33. Singer, A.; Johst, K.; Banitz, T.; Fowler, M.S.; Travis, J.M.J. Community dynamics under environmental change: How can next generation mechanistic models improve projections of species distributions. *Eco. Model.* **2016**, *326*, 63–74. [[CrossRef](#)]
34. Schmidt, J.; Ian, E.S.; Brinkmann, J. Comparison of polynomial models for land surface curvature calculation. *Int. J. Geogr. Inf. Sci.* **2003**, *17*, 797–814. [[CrossRef](#)]
35. Meng, B.P.; Liang, T.G.; Yi, S.H.; Yin, J.P.; Cui, X.; Ge, J.; Hou, M.J.; Lv, Y.Y.; Sun, Y. Modeling alpine grassland above ground biomass based on remote sensing data and machine learning algorithm: A case study in the east of Tibetan Plateau, China. *IEEE J. Sel. Top. Appl. Earth Obs. Remote Sens.* **2020**, *13*, 2986–2995. [[CrossRef](#)]
36. Yuan, M.L.; Zhang, Q.L.; Zhang, L.; Jia, C.L.; Li, X.P.; Yang, X.Z.; Feng, R.Q. Mitochondrial phylogeny, divergence history and high-altitude adaptation of grassland caterpillars (Lepidoptera: Lymantriinae: Gynaephora) inhabiting the Tibetan Plateau. *Mol. Phylogenet. Evol.* **2018**, *122*, 116–124. [[CrossRef](#)]
37. Shi, D.Z.; Yun, X.J. Improvement of the grassland early pest warning system. *Grassl. J.* **2005**, *13*, 71–74.
38. Ziolkowska, E.; Topping, C.J.; Bednarska, A.J.; Laskowski, R. Supporting non-target arthropods in agroecosystems: Modelling effects of insecticides and landscape structure on carabids in agricultural landscapes. *Sci. Total Environ.* **2021**, *774*, 145746. [[CrossRef](#)]
39. Li, C.; Connor, T.; Bai, W.K.; Yang, H.B.; Zhang, J.D.; Qi, D.W. Dynamics of the giant panda habitat suitability in response to changing anthropogenic disturbance in the Liangshan Mountains. *Biol. Conserv.* **2019**, *237*, 445–455. [[CrossRef](#)]
40. Kukal, O.; Heinrich, B.; Duman, J.G. Behavioural thermoregulation in the freeze tolerant arctic caterpillar, *Gynaephora groenlandica*. *J. Exp. Biol.* **1988**, *138*, 181–193. [[CrossRef](#)]
41. Bennett, V.A.; Lee, R.E.; Nauman, J.S.; Kukal, O. Selection of overwintering microhabitats used by the arctic wool-lybear caterpillar, *Gynaephora groenlandica*. *Cryoletters* **2003**, *24*, 191–200.
42. Wang, H.Z.; Liu, X. Distribution of *Gynaephora qinghaiensis* population and its effect on habitat grassland vegetation in Yushu Prefecture. *J. Environ. Entomol.* **2022**, *44*, 12. [[CrossRef](#)]
43. Yu, J.L.; Shi, H.X. Effects of grassland caterpillars on the plant community structure of alpine Kobresia meadows and soil properties. *J. Anhui Agric. Sci.* **2010**, *38*, 62–64. [[CrossRef](#)]
44. Strathdee, A.T.; Bale, J.S. Life on the edge: Insect ecology in arctic environments. *Annu. Rev. Entomol.* **1998**, *43*, 85–106. [[CrossRef](#)]
45. Yan, L. Studies of Taxonomy, Geographic Distribution in *Gynaephora* Genus and Life-History Strategies on *Gynaephora Menyuanensis*. Ph.D. Thesis, Lanzhou University, Lanzhou, China, 2006.
46. Gao, Y.Y.; Ma, Q.S.; Zhang, X.Y.; Ma, J.H.; Yi, S.H.; Li, B.C.; Zhang, J.G.; Lu, X.M.; Sun, Y. Preliminary exploration of monitoring *Gynaephora alpherakii* using unmanned aerial vehicles (UAV). *Pratac. Sci.* **2020**, *37*, 2106–2114. [[CrossRef](#)]
47. Lv, Y.Y.; Zhao, X.Q.; Zhang, S.R.; Zhang, J.G.; Yue, K.T.; Meng, B.P.; Li, M.; Cui, W.X.; Sun, Y.; Zhang, J.G.; et al. Herbaceous dominant the changes of normalized difference vegetation index in the transition zone between desert and typical steppe in Inner Mongolia, China. *Front. Plant Sci.* **2022**, *12*, 3415. [[CrossRef](#)]
48. Yi, S.H. FragMAP: A tool for long-term and cooperative monitoring and analysis of small-scale habitat fragmentation using an unmanned aerial vehicle. *Int. J. Remote Sens.* **2017**, *38*, 2686–2697. [[CrossRef](#)]
49. Zhang, J.G.; Liu, D.W.; Meng, B.P.; Chen, J.J.; Wang, X.Y.; Jiang, H.; Yu, Y.; Yi, S.H. Using UAVs to assess the relationship between alpine meadow bare patches and disturbance by pikas in the source region of Yellow River on the Qinghai-Tibetan Plateau. *Glob. Ecol. Conserv.* **2021**, *26*, e01517. [[CrossRef](#)]

**Disclaimer/Publisher’s Note:** The statements, opinions and data contained in all publications are solely those of the individual author(s) and contributor(s) and not of MDPI and/or the editor(s). MDPI and/or the editor(s) disclaim responsibility for any injury to people or property resulting from any ideas, methods, instructions or products referred to in the content.